LA-UR -80-2854

TITLE: NUMERICAL CALCULATION OF SHOCK-INDUCED INITIATION OF DETONATIONS

AUTHOR(S): G. Edward Cort
Jerry H. Fu

SUBMITTED TO: JANNAF Intragency Propulsion Committee, 1980 Propulsion Systems Hazards Meeting, Monterey, California, October 27-31, 1980.

MASTER

University of California

LOS ALAMOS SCIENTIFIC LABORATORY
Post Office Box 1663 Los Alamos, New Mexico 87545
An Affirmative Action/Equal Opportunity Employer

NUMERICAL CALCULATION OF SHOCK-INDUCED INITIATION OF DETONATIONS*

G. E. Cort and J. H. M. Fu
Los Alamos Scientific Laboratory
Los Alamos, New Mexico

ABSTRACT

This paper describes the results of some numerical calculations of the impact of steel cylinders and spheres on the plastic-bonded high explosive PBX 9501. The calculations were carried out by a reactive, multicomponent, two-dimensional, Eulerian hydrodynamic computer code, 2DE. The 2DE computer code is a finite difference code that uses the donor-acceptor-cell method to compute mixed cell fluxes.

The mechanism of shock initiation to det nation in heterogeneous explosives is best described as local decomposition at hot spots that are formed by shock interactions with density discontinuities. The liberated energy strengthens the shock so that as it interacts with additional inhomogeneities, hotter hot spots are formed, and more of the explosive is decomposed. The shock wave grows stronger until a detonation begins. This mechanism of initiation has been described numerically by the Forest Fire burn model, which gives the rate of explosive decomposition as a function of local pressure. The parameters in the Forest Fire burn model have been developed from experiments where the induced shock approximates a plane wave and are applied, in this case, to a situation where the induced shock is a divergent wave with curvature that depends on the size and shape of the projectile.

The calculated results have been compared with results from experiments involving instrumented mock and live high explosives, with projectiles of varying sizes, shapes, and velocities. We find that there is good agreement between the calculated and experimental data.

INTRODUCTION

A major problem in the handling and storage of munitions, and of explosive materials in general, is the possibility of the propagation of detonations from a damaged warhead or motor into nearby explosive objects. Because modern high-specific impulse solid fuels are composed mainly of explosive substances, concern with problems of sympathetic detonation has increased. This sympathetic detonation phenomenon can be caused by the blast from the primary explosion or by the impact of debris fragments.

*This work was supported by the US Department of Energy, Office of Military Applications. We gratefully acknowledge the assistance and contributions of C. L. Mader, C. A. Forest, A. L. Bowman, J. D. Kershner, L. A. Gritzo, and L. W. Hantel. The instrumented projectile impact experiments were performed by G. A. Carlson, T. R. King, R. J. DeWitt, J. A. Sanchez, and K. C. Pederson; the uninstrumented experiments were performed by J. A. Sanchez and K. C. Pederson.

This study concentrates on impact by simulated steel debris fragments on PBX 9501, a mixture of 95% HMX-2, 2.5% nitroplasticizer, and 2.5% Estane by weight. The approach used here could be applied with more typical rocket propellants. to determine critical debris particle sizes and velocities that would not cause a detonation.

The shock initiation of a detonation refers to a process in which a shock wave induced in an explosive charge develops into a propagating detonation wave. In many experimental studies, the induced shock is generated by a plane-wave lens or by a flying plate whose characteristic length is larger than or is comparable to that of the explosive sample. In those studies, the assumption that the induced shock is a plane wave is a reasonable approximation before the arrival of the unloading rarefaction waves. The plane-wave approximation has been used in the sensitivity studies of many explosives. The well-known Pop plots for a variety of explosives are the result of those studies. The Pop plot of an explosive is a sensitivity indicator that expresses the distance of run to detonation as a function of the initial pressure.

When a small projectile strikes a high explosive (HE) sample, the propagating shock wave may decay and die, failing to initiate a detonation, or it may be amplified and initiate a detonation in the explosive. The decay of the wave is caused by rarefaction waves from interfaces and by the geometric-divergence effect: both weaken the shock. On the other hand, the propagating shock interacts with density discontinuities to create local hot spots.[1,2] The energy released from the shock-induced decomposition of the explosive at hot spots strengthens the shock. If the strengthening process prevails, a detonation will result. Thus, the shock initiation in an explosive struck by a projectile depends on the type and configuration of the target explosive and the material, velocity, and shape of the incident projectile.

EXPERIMENTS

The numerical study and accompanying experiments involved a single type of test. The projectiles were fired from a gas gun at a small block of PBX 9501 or 900-10 mock (1.867 g/cm^3 (116.7 lbm/ft^3) density) explosive. The 900-10 and some of the PBX 9501 blocks were instrumented with carbon and Manganin gauges to measure pressure and Constantan gauges to measure strains. The gauges were located on-axis at 17 mm (0.67 in.) and 34 mm (1.34 in.) from the impact surface and 10 mm (0.39 in.) off-axis at 17 mm (0.67 in.) from the impact surface. A summary of the results that are used as a basis for comparison with the numerical calculations is given in Table I.

For 7.62 mm (0.30 in.)-diam steel cylinders impacting at 845 m/s (2772 ft/s) on 900-10, the peak shock pressures measured at 17 mm (0.67 in.) and 34 mm (1.34 in.) on-axis were 0.2 ± 0.03 and 0.06 ± 0.015 GPa (2.0 ± 0.3 and 0.60 ± 0.15 kbar), respectively. For the same impact on PBX 9501, the average pressures were about a factor of 8 higher because of the low-order reactions in the HE, but a full detonation did not occur. The uninstrumented PBX 9501 detonated on impact at 873 m/s (2864 ft/s) with the same projectile. A cylindrical projectile almost half the diameter

TABLE I

SUMMARY OF EXPERIMENTAL RESULTS

I. Instrumented Targets, PBX 9501 and 900-10 (~ 1 m Range)
7.62 mm diam x 15.24 mm long (0.30 in. diam x 0.60 in. long) steel cylinders at 845 ± 10 m/s (2772 ± 33 ft/s).[a]

Shot No.	Target	Peak Shock Pressure (GPa)[b] On Axis 17 mm (0.67 in.)	On Axis 34 mm (1.34 in.)	10 mm (0.39 in.) Off Axis 17 mm (0.67 in.)
1.	900-10	0.230	0.05	0.160
2.	900-10	0.200	0.07	0.130
3.	900-10	0.170	-	-
4.	900-10	0.140	0.07	-
5.	PBX 9501	1.250	0.41	0.900
6.	PBX 9501	1.670	-	1.550
AVG	900-10	0.20 ± 0.03	0.060 ± 0.015	0.145 ± 0.02
AVG	PBX 9501	1.530 ± 0.25	0.410	1.220 ± 0.350

II. Uninstrumented Targets, PBX 9501 (12 m Range)

Shot No.	Steel Projectile Size, mm (in.) Shape	Velocity, m/s (ft/s)	Result[c]
1-7	6.35 (0.25) diam sphere	1238 to 2506 (4062 to 8222)	No go
8	7.62 (0.30) diam cylinder x 15.2 (0.60) long	873 (2864)	Go
9	3.35 (0.13) diam cylinder x 6.71 (0.26) long	2275 (7464)	Go
10	3.35 (0.13) diam cylinder x 6.71 (0.26) long	2093 (6867)	No go
11	3.35 (0.13) diam cylinder x 6.71 (0.26) long	2178 (7146)	Go
12-15	7.94 (0.31) diam sphere	1700 to 1850 (5577 to 6070)	No go

[a]All projectiles struck the PBX 9501 surface at 0° obliquity, within 5 mm (0.20 in.) of centerline.

[b]1 GPa = 10 kbar.

[c]Go = detonation.

caused a detonation at 2178 m/s (7146 ft/s), but not at 2093 m/s (6867 ft/s).

No detonations were observed with 7.94 mm-diam (0.31 in.) spherical projectiles at velocities to 1.85 km/s (6070 ft/s). Spherical projectiles 6.35 mm (0.25 in.) in diam did not cause detonations at velocities up to 2.506 km/s (8222 ft/s).

MODEL

The computation of sympathetic detonation from projectile impact was performed with the two-dimensional Eulerian reactive hydrodynamic code, 2DE,[2,3] using the Forest Fire burn rate.[1,2] The equation-of-state data used in these calculations are given in Appendix A. The Forest Fire burn rate parameters and Pop plot data are given in Appendix B. The Pop plots for PBX 9501 and PBX 9404* are given in Fig. 1. The density of the PBX 9501 used in these experiments and computations was 1.833 g/cm^3 (114.6 lb$_m$/ft^3). PBX 9501 is slightly less sensitive than PBX 9404. The scatter in the experimental data for PBX 9501 gives an indication of the relative error in our calculated results. The partially reacted Hugoniots are given in Fig. 2 for 900-10, PBX 9501, and PBX 9404.

The configuration of the explosive target in the computer model is cylindrical with the centerlines of the projectile and target coincident (Fig. 3). Typical mesh dimensions and numbers of computational cells are given in the R and Z directions.

An important parameter in numerical modeling of shock waves is the artificial viscosity used in finite-difference solutions to smear out the shock. Without artificial viscosity, the step changes in pressure and temperature across the shock can occur within a single mesh cell and make the numerical solution unstable. There is no *a priori* method of determining the best value of the artificial viscosity for any given problem, although the shock must be smeared across a few mesh cells for stability. If the artificial viscosity is too large, the shock pressure will be reduced. This would be particularly serious in the present study because the Forest Fire burn rate would also be affected by the incorrect pressure. The numerical model was calibrated by ensuring that the artificial viscosity was small enough that the numerical model predicted the measured pressures in the experiments.

RESULTS

900-10

For the cylinder impact corresponding to the experimental conditions, Table II gives the calculated peak shock pressures corresponding to the measurement locations.

*Composition of PBX 9404 is 94% HMX, 3% nitrocellulose, and 3% tris-β-chloroethyl phosphate.

TABLE II

PEAK SHOCK PRESSURE IN 900-10
Struck by 7.62 mm (0.30 in.) diam Cylinder
at 845 m/s (2772 ft/s).

Location	Peak Pressure, GPa[a]	
	Measured	Calculated
On axis, Z = 17 mm (0.67 in.)	0.200 ± 0.03	0.235
Off axis, Z = 17 mm (0.67 in.)	0.145 ± 0.02	0.205

[a]1 GPa = 10 kbar.

A series of pressure profiles (Fig. 4) taken along the axis at various times after impact, shows that the leading edge of the shock wave is fairly sharp and extends across several mesh cells. The artificial viscosity used for this case is 0.25. Figure 5 shows isobars at about 2 μs after impact, indicating the curvature caused by rarefactions and divergence.

PBX 9501

The same calculational model was used for the PBX 9501 except for the properties. The impact velocity was again 845 m/s (2772 ft/s). Table III gives the comparison between the average experimental and calculated peak shock pressures. Although considerable decomposition of the HE took place, there was no detonation in either the experiment or the calculation. Figure 6 shows the shock pressure and the unburned mass fraction versus distance (cell number) along the Z axis. The increase in peak pressure over that observed with 900-10 is a consequence of the energy released by chemical decomposition of the PBX 9501. The curvature in the shock wave is essentially identical to that observed with 900-10 (Fig. 7).

TABLE III

PEAK SHOCK PRESSURE IN PBX 9501
Struck by 7.62 mm (0.30 in.)-diam cylinder
at 845 m/s (2772 ft/s).

Location	Peak Pressure, GPa[a]	
	Measured	Calculated
On axis, Z = 17 mm (0.67 in.)	1.530 ± 0.25	1.480
Off axis, Z = 17 mm (0.67 in.)	1.220 ± 0.350	1.160

[a]1 GPa = 10 kbar.

The calculation was then repeated with identical parameters except that the cylinder velocity was increased to 873 m/s (2864 ft/s). A full detonation occurred after a run of 7.14 mm (0.28 in.). Based on an initial pressure of 5.5 GPa (55 kbar) from matched Hugoniots for steel and unreacted PBX 9501, the Pop plot indicates a run to detonation of 4.52 mm

(0.18 in.). The increased distance to detonation can be attributed to the decay in shock pressure with divergence. Figure 8 shows isobars and contours of constant mass fraction for times just before and just after the start of detonation, 50 computational cycles, or less than 0.5 μs apart. The corresponding pressure profiles and mass fractions versus distance along the centerline are shown in Fig. 9. The shock pressure is increasing with time as the detonation builds up behind it. Eventually, a steady detonation wave will be reached with peak pressure equal to 33.5 GPa (335 kbar), slightly less than that of the Chapman-Jouguet point.

Cylinder, 3.35 mm (0.13 in.)-diam

Much higher velocities were required to cause a detonation in the experiments with the smaller cylinder. The same computational model was used, except that the mesh size was reduced to help resolve parameters on the smaller scale. The behavior of the explosive is quite different than described previously for the larger cylinder. Figure 10 shows the peak pressure in the explosive plotted as a function of time after the impact for three different sets of conditions:

1. Impact at 2.093 km/s (6867 ft/s) with the chemical reaction in the explosive turned off.

2. Impact at 2.093 km/s (6867 ft/s) with the Forest Fire burn model (reaction turned on).

3. Impact at 2.178 km/s (7146 ft/s) with the Forest Fire burn model.

In the first case, the peak pressure does not equal the 18.4 GPa (184 kbar) predicted from matched Hugoniots for the nonreacted HE and steel. In the second case, the pressure rises in about 0.3 μs to about 28 GPa (280 kbar) because of the reaction, but again falls off. Some of the computational cells near the centerline and the impact interface are completely reacted, a condition that ordinarily (in one-dimensional computations or in those just described for the larger cylinder) would propagate into a high-order detonation. In this case, the projectile is small enough that side rarefactions quickly reduce the peak pressure and the explosive does not detonate, in agreement with experimental observations. As a matter of interest, the failure diameter for PBX 9404 is 1.20 ± 0.2 mm (0.047 ± 0.008 in.), about 35 % of the projectile's diameter. The failure diameter for PBX 9501 has not been determined, but should be approximately the same. In the third case, the peak pressure rises to about 28 GPa (280 kbar) in the first 0.3 μs and falls to about 14 GPa (140 kbar) about 1.0 μs after that. However, because the energy released in the chemical reaction is enough to overcome the effect of the side rarefactions, the peak pressure increases again and a full detonation results.

The isobars and contours of constant mass fraction for the latter two cases are compared in Fig. 11.

Sphere, 6.35 mm (0.25 in.)-diam

The impact of the steel sphere with the PBX 9501 was calculated for one velocity, 1852 m/s (6077 ft/s). Recall that the experiments determined that no detonation occurred for seven tests with impact velocities ranging from 1.238 to 2.506 km/s (4062 to 6745 ft/s). The isobars at 0.20 μs and 1.58 μs after impact are shown in Fig. 12. The effect of rarefactions can be seen at the sphere-HE interface. The peak pressure reached in this case is only 11 GPa (0.11 Mbar) versus 15.4 GPa (0.154 Mbar) that is predicted from matched Hugoniots for nonreacting explosive and steel.

CONCLUSIONS

The shock-induced detonation of small samples of PBX 9501 by the impact of projectiles of different shapes and sizes has been modeled successfully. The results of the calculations are in good agreement with experimental observations. We can predict other results from considerations of projectile velocity, size, shape, and explosive properties.

The curvature of the impact-induced shock wave caused by side rarefactions and geometric divergence is the major difference between this class of shock-induced detonation and that caused by a plane-wave lens or flyer plate. These effects cannot be scaled easily because of nonlinear interactions.

APPENDIX A

EQUATION OF STATE

The HOM equation of state is used to solve for pressure P and temperature T in a cell, with specific volume V and specific internal energy I as input. The shock velocity U_S and the particle velocity U_p are related by

$$U_S = C + SU_p.$$

The equations for a solid are

$$P_H = C^2(V_0 - V)/[V_0 - S(V_0 - V)]^2$$

$$X = \ln V$$

or $$T_H = F + GX + HX^2 + IX^3 + JX^4$$

$$I_H = (1/2)\, P_H(V_0 - V)$$

$$P = (\gamma/V)\,(I - I_H) + P_H$$

$$T = (I - I_H)\,(23\,890)/C_V + T_H$$

The equations for a gas are

$$X = \ln V$$

$$Y = \ln P_i$$

$$Y = A + BX + CX^2 + DX^3 + EX^4$$

$$\ln I_i = K + LY + MY^2 + NY^3 + OY^4$$

$$I_i = I_i - Z$$

$$\ln T_i = Q + RX \quad SX^2 + TX^3 + UX^4$$

$$-1/\beta = R + 2SX + 3TX^2 \; 4UX^3$$

$$P = [1/(\beta V)] (I - I_i) + P_i$$

$$T = (I - I_i) (23\ 890) C_V' + T_i$$

The solution for a cell with more than one component is based on combinations of these equations.[2,3]

The equation-of-state parameters used in this study are tabulated in Table A-I. The units are volume (cm^3/g), energy ($Mbar\text{-}cm^3/g$), pressure (Mbar), temperature (K), velocity (cm/μs), and heat capacity (cal/g-K).

TABLE A I

EQUATION OF STATE PARAMETERS

PBX 9501

C	2.500000000000E-01	D	3.043215493500E-02
S	2.180000000000E+00	E	-1.632553561600E-02
F	-1.736298901400E+01	K	-1.612213734400E+00
G	-1.111079475900E+02	L	5.275117547200E-01
H	-1.941853902200E+02	M	7.024394327500E-02
I	-1.418535926800E+02	N	4.643524952000E-03
J	-3.359704507400E+01	O	1.234139635400E-04
γ	1.500000000000E+00	P	7.366260658300E+00
C_V	3.000000000000E-01	R	-5.086700168300E-01
ν	5.455537370400E-01	S	3.553568750600E-02
α	1.000000000000E-04	T	3.942242644100E-02
A	-3.525872840600E+00	U	-1.367380827300E-02
B	-2.602094152600E+00	C_V'	5.000000000000E-01
C'	2.615657058600E-01	Z	1.000000000000E-01

Steel

C	4.580000000000E-01	J	-1.663916159830E+03
S	1.510000000000E+00	γ	2.000000000000E+00
F	-3.823825874530E+03	C_V	1.070000000000E-01
G	-7.032119540240E+03	ν	1.263104711000E-01
H	-4.826702138900E+03	α	1.170000000000E-05
I	-1.466784021180E+03		

TABLE A-1. EQUATION OF STATE PARAMETERS - CONTINUED

Air

A	-4.50602542688E+00	D	-1.58521895338E-06
B	-1.27546110628E+00	R	8.22644581441E+00
C'	-3.74276600292E-03	R	-2.51525130950E-01
D	1.23929236747E-02	S	-1.34446940047E-02
E	-2.07694122929E-03	T	1.40871016422E-02
K	-1.62655447438E+00	U	-2.18132189985E-03
L	9.05283146618E-02	C_V'	5.00000000000E-01
M	2.69004997726E-03	Z	1.00000000000E-01
N	-5.43583122192E-05	V	8.65224000000E+02

APPENDIX B

FOREST FIRE BURN RATE

The mass fraction of unburned explosive W is defined as W = 1 for pure solid, and burns to gaseous products, W = 0, according to a pressure-dependent rate law based on experimental data.[1,2] The rate R is defined for pressure P in Mbars and time t in μs by

$$R = (1/W)\ (dW/dt),$$

$$\ln R = \sum_{i=1}^{N} C_i P^{i-1} .$$

The limiting conditions set R = 0 for P less than a specified cutoff pressure and R = ∞ (W > 0 immediately) when P reaches the C-J pressure. The rate parameters used in this study are tabulated in Table B-I.

TABLE B-I

FOREST FIRE RATE PARAMETERS

PBX 9501

C-J PRESSURE = 0.3595 CUT-OFF PRESSURE = 0.005

C(I=1,14) =

-9.8934158B60E+00	9.065003C181E+02	-1.8867412C6E+04
9.0905952790E+05	-9.4510342786E+06	1.2276466725E+08
-1.1353446359E+09	7.5536596868E+09	-3.6199460533E+10
1.2371591489E+11	-2.9390384021E+11	4.60E7898934E+11
-4.2871378222E+11	1.79099750P6E+11	

These Forest Fire parameters are derived from the experimentally determined Pop plots. The equation of the Pop plot is

$$\ln x = A + B \ln P,$$

with the run distance x in cm and the pressure P in Mbars. The Pop plots are shown in Fig. 1. The parameters are given in Table B-II.

TABLE B-II

POP-PLOT PARAMETERS

	A	B
PBX 9501	-5.0827BB910	-1.475245725

REFERENCES

1. C. L. Mader and C. A. Forest. "Two-Dimensional Homogeneous and Heterogeneous Detonation Wave Propagation," Los Alamos Scientific Laboratory report LA-6259 (1976).

2. C. L. Mader, "Numerical Modeling of Detonations" (University of California Press, Berkeley, 1979).

3. J. D. Kershner and C. L. Mader, "2DE, A Two-Dimensional Continuous Eulerian Hydrodynamic Code for Computing Multicomponent Reactive Hydrodynamic Problems," Los Alamos Scientific Laboratory report LA-4846 (March 1972).

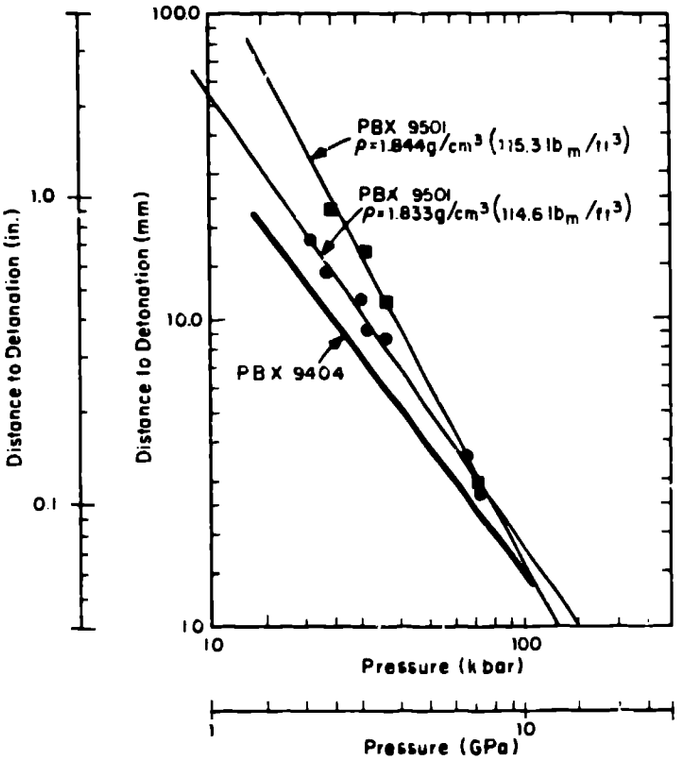

Figure 1. Pop Plots for PBX 9501 and PBX 9404

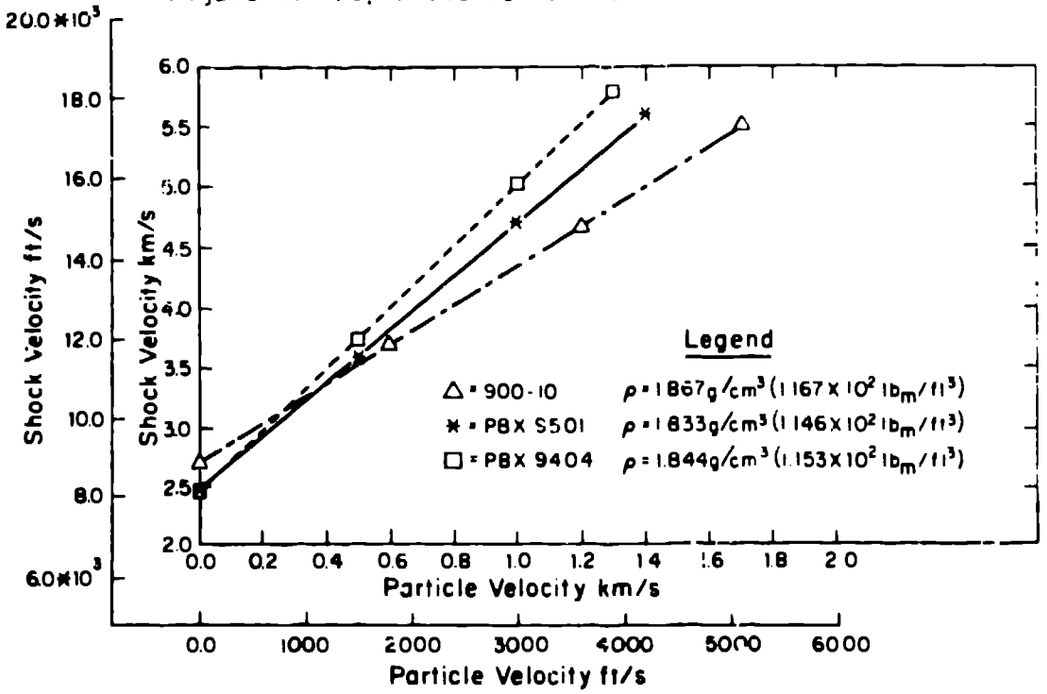

Figure 2. Shock-Particle Velocity Relation for 900-10, PBX 9501, and PBX 9404

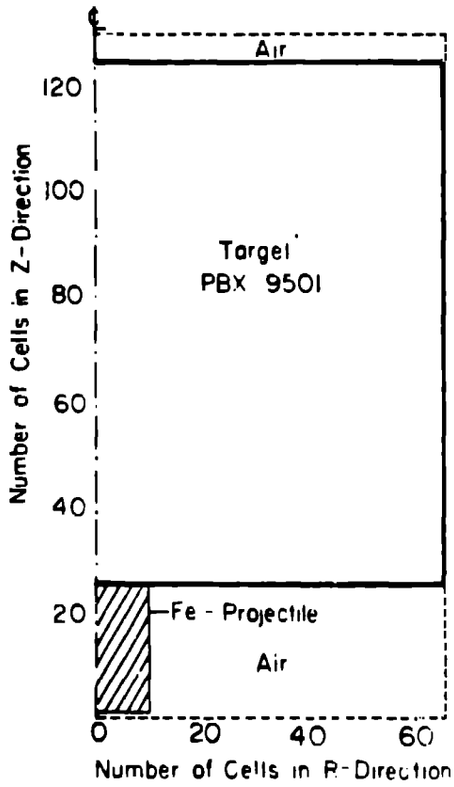

Figure 3. Typical Computer Model for an Impinging Cylindrical Projectile

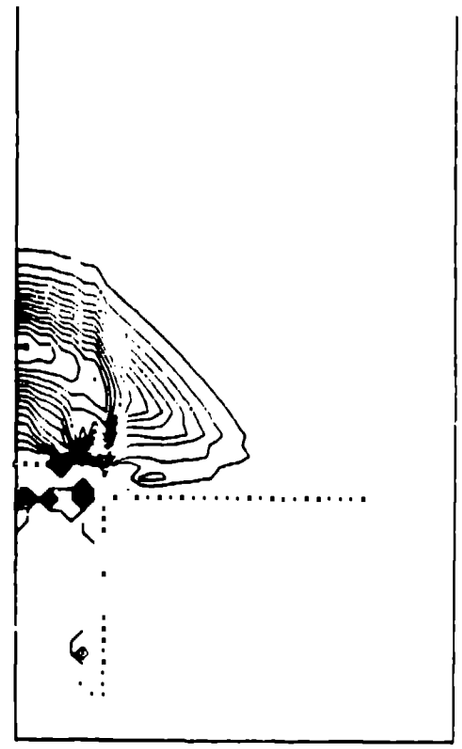

Figure 5. Calculated Isobars in 900-10 at 1.91 μs After Impact by 7.62 mm (0.30 in.)-diam Cylinder at 845 m/s (2772 ft/s)

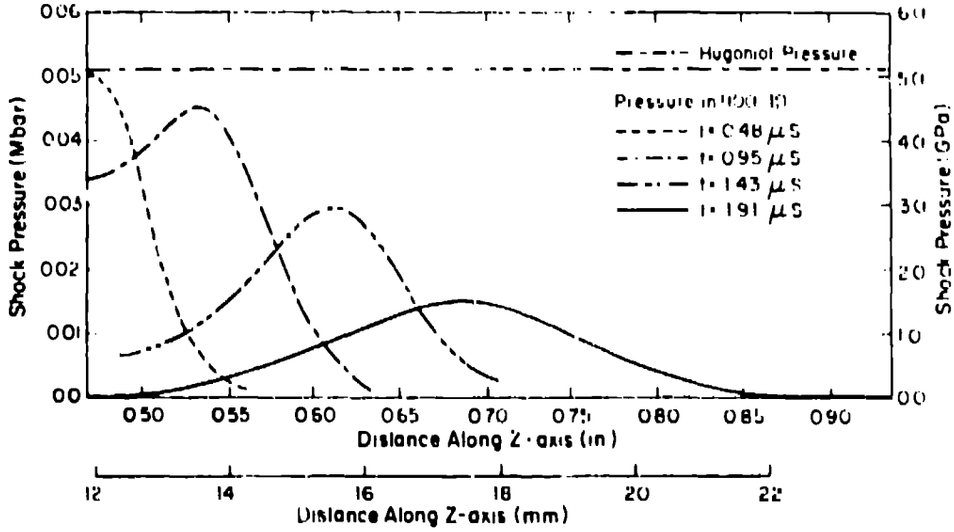

Figure 4. Calculated Pressure Along Centerline for 7.62-mm (0.30 in.)-diam Cylinder Impact on 900-10 at 845 m/s (2772 ft/s) at Various Times After Impact

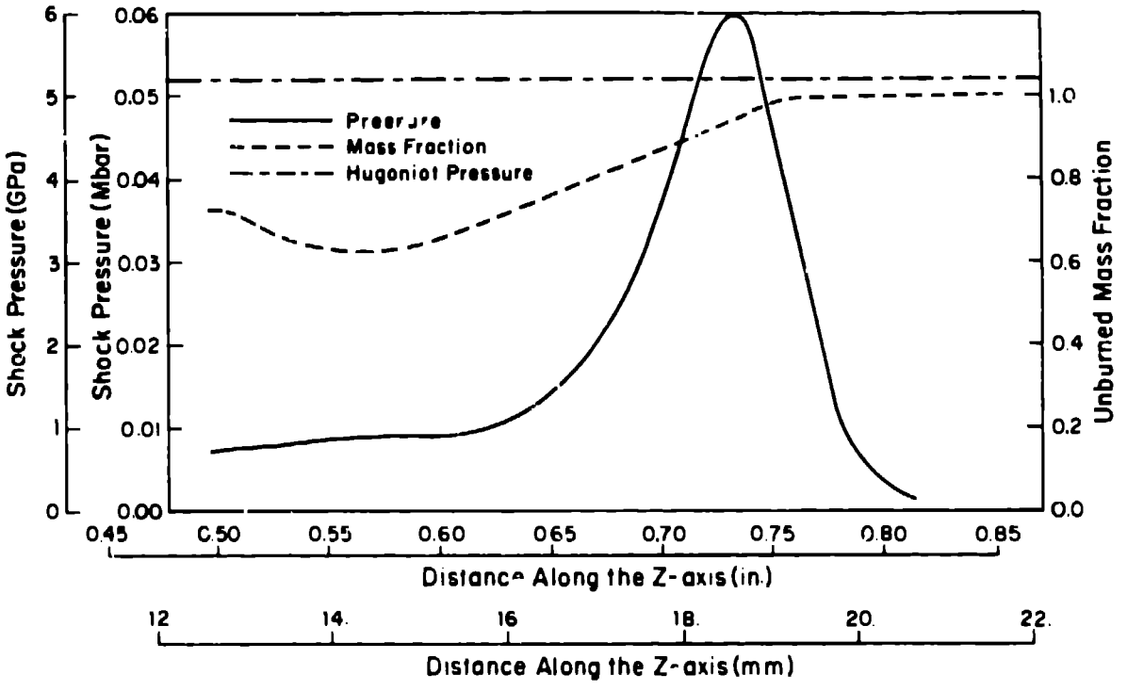

Figure 6. Calculated Pressure and Unburned Mass Fraction for 7.62 mm (0.30 in.)-diam Cylinder Impact on PBX 9501 at 845 m/s (2772 ft/s), 1.91 μs After Impact

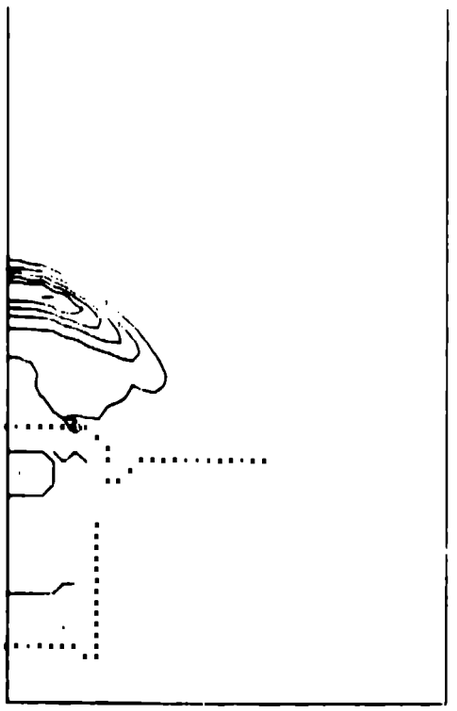

Figure 7. Calculated Isobars in PBX 9501 at 1.91 μs After Impact by 7.62 mm (0.30 in)-diam Cylinder at 845 m/s (2772 ft/s)

Figure 8. Isobars (Top) and Contours of Constant Mass Fraction at 1.91 μs (Left) and 2.38 μs After Impact by 7.62 mm (0.30 in.) Cylinder at 873 m/s (2864 ft/s)

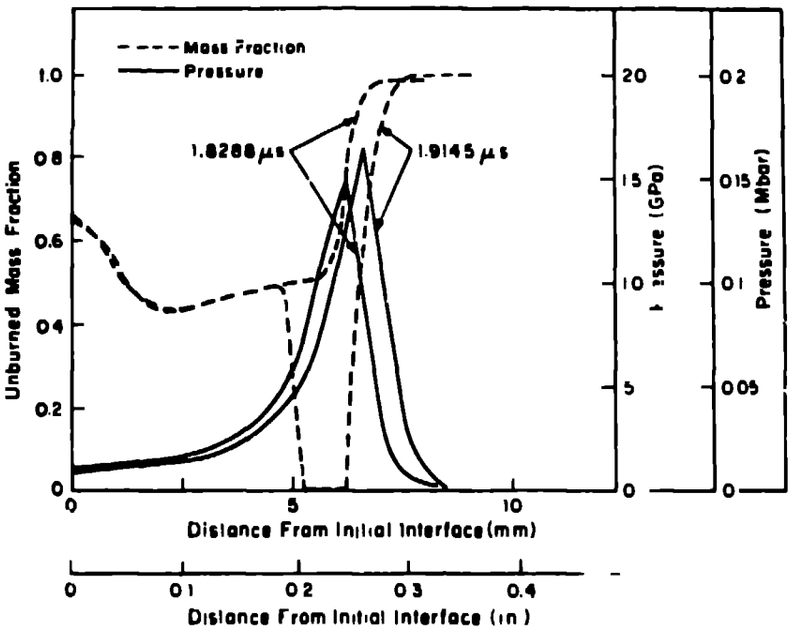

Figure 9. Pressure and Unburned Mass Fraction for 7.62 mm (0.30 in.)-diam Cylinder Impact at 873 m/s (2864 ft/s)

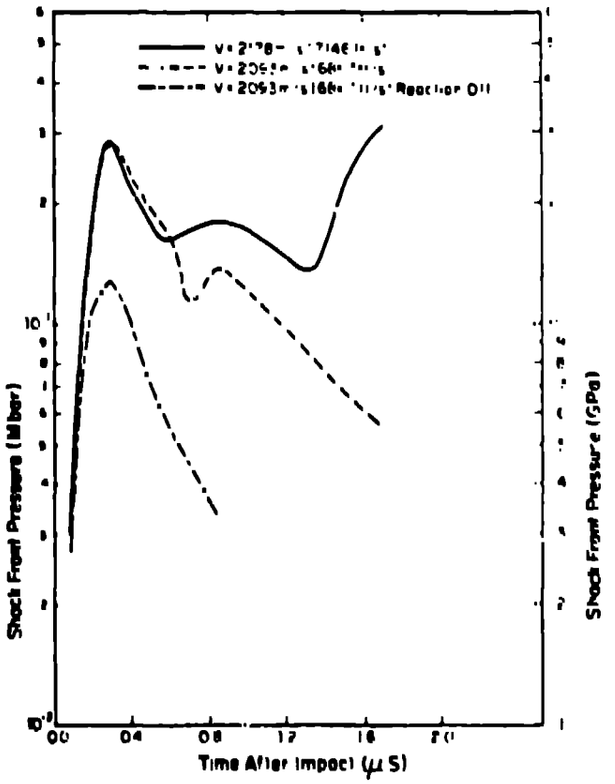

Figure 10. Shock Front Pressure versus Time for Impact by 3.35 mm (0.13 in.)-diam Cylinder

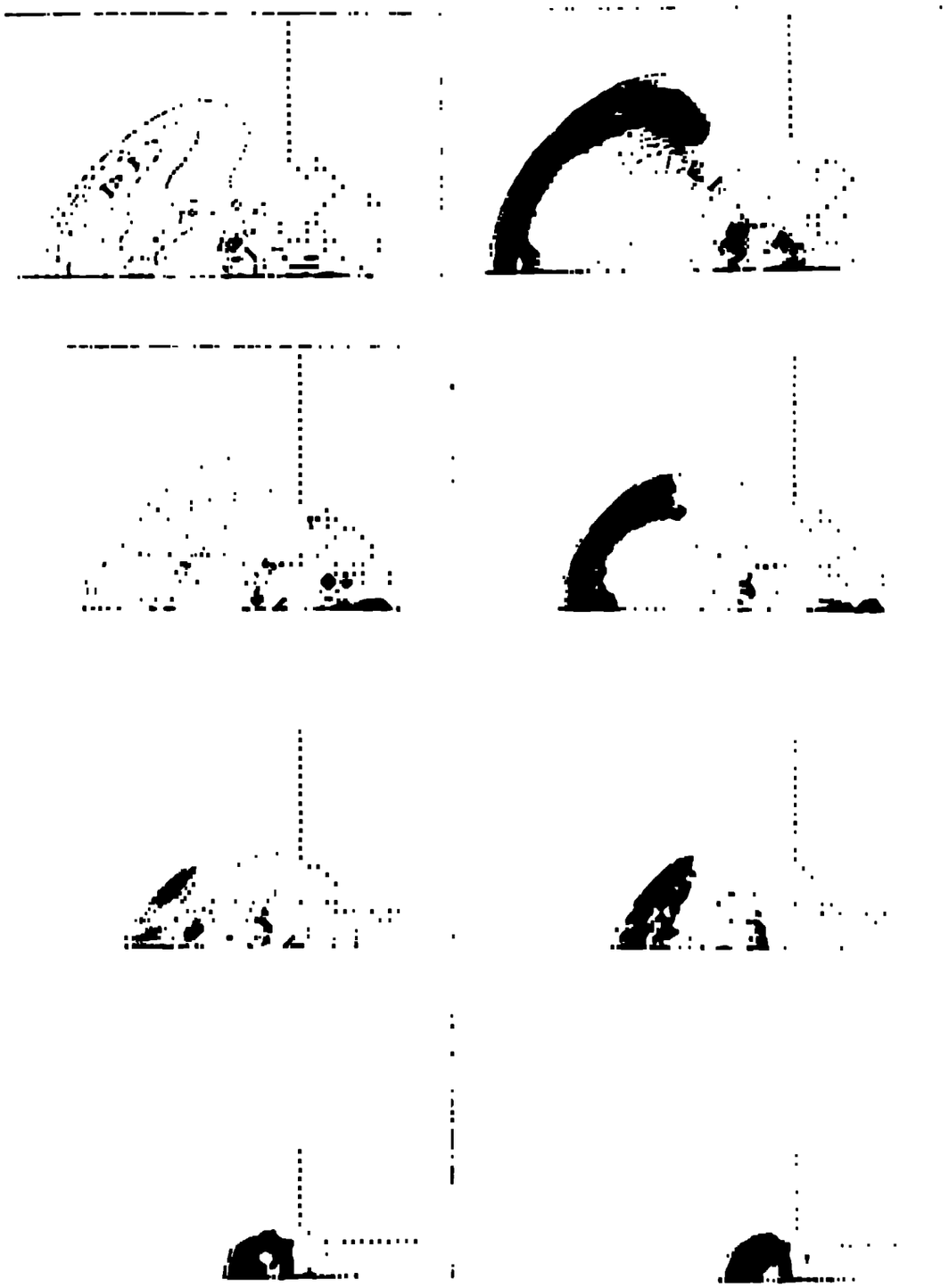

Figure 11a. Isobars Following Impact of 3.35 mm (0.13 in.)-diam Cylinder at 2093 m/s (6867 ft/s) at Top and 2172 m/s (7126 ft/s), at Bottom at 0.42, 1.26, 1.68, and 2.1 ms

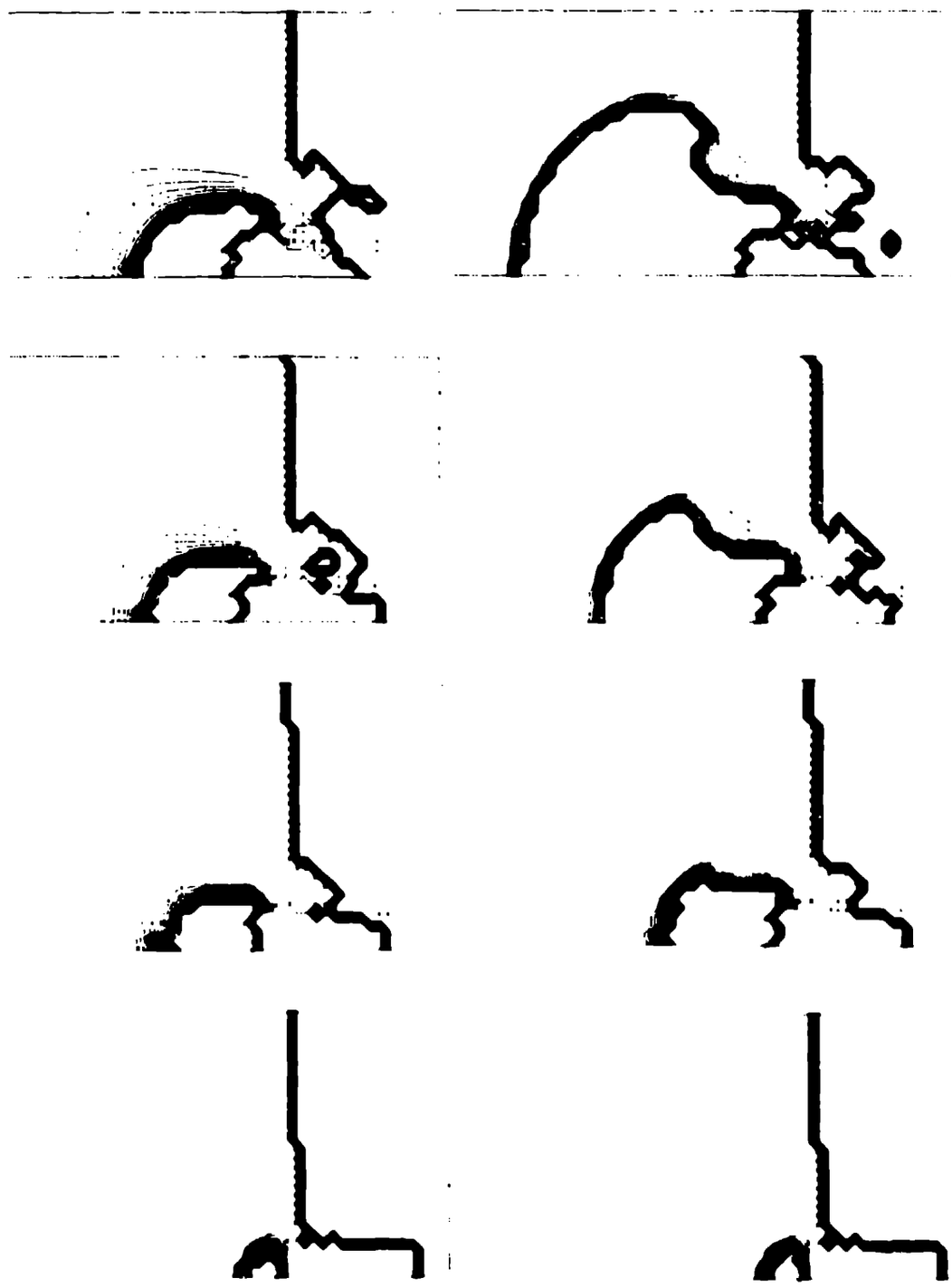

Figure 11b. Contours of Constant Mass Fraction Following Impact of 3.30 mm (0.13 in.)-diam Cylinder at 2093 m/s (6967 ft/s), at Top and 2178 m/s (7146 ft/s). at Bottom at 0.42, 1.26, 1.68, and 2.1 μs

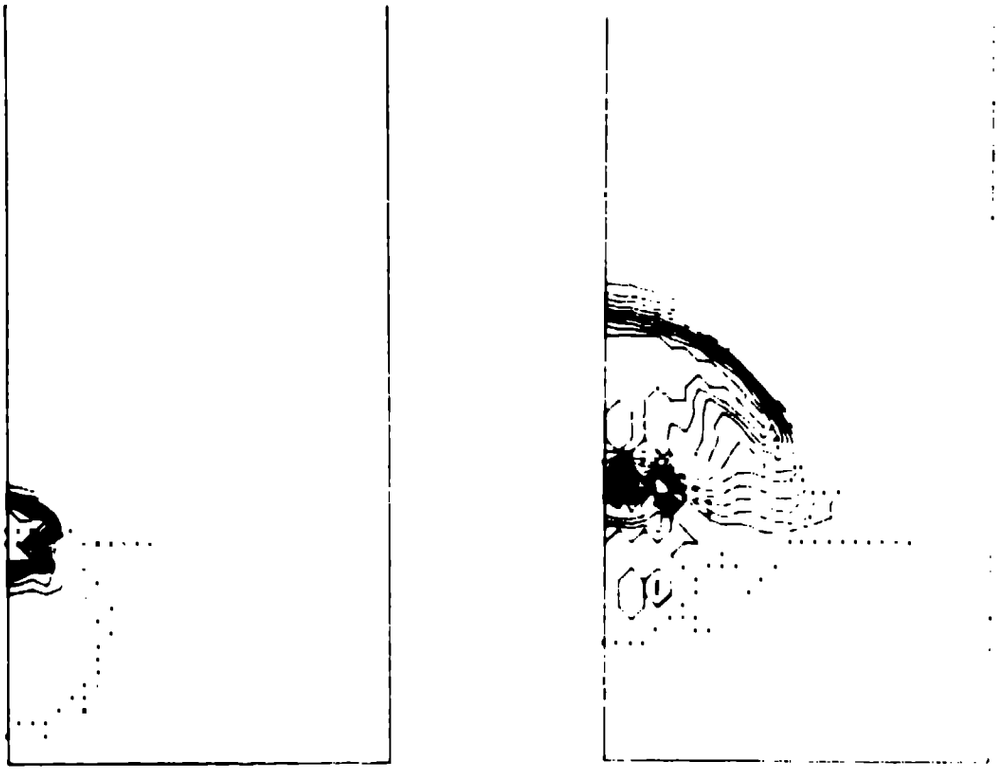

Figure 12. Isobars at 0.20 μs and 1.58 μs After Impact with 6.35 mm (0.25 in.)-diam sphere at 1852 m/s (6077 ft/s)